Kinetic study of the low temperature internal oxidation of nickel based model alloys exposed to PWR primary water

Benoît Ter-Ovanessian[1,2, a] Julien Deleume[1, b],' Jean-Marc Cloué[1, c], Eric Andrieu[2, d]

[1] AREVA, AREVA NP 10, rue J. Récamier, 69456 Lyon Cedex 06, France

[2] CIRIMAT, CNRS/UPS/INPT, ENSIACET, 118, route de Narbonne, 31077 Toulouse Cedex 4, France

[a]benoit.terovanessian@ensiacet.fr, [b]julien.deleume@areva.com, [c]jean-marc.cloue@areva.com, [d]eric.andrieu@ensiacet.fr

Keywords : Corrosion, Nickel alloys, STEM, SIMS, Grain boundary embrittlement

Abstract. Two Ni-Fe-Cr ternary alloys have been oxidized in simulated pressurized water reactor primary water at 360°C for 1000 h. The chemical composition of those alloys were chosen in order to be representative of the one of chromium depleted areas under the oxide scale of industrial alloys (e.g. alloy 600) exposed in the same conditions. The resulting oxidized structures (corrosion scale and underlying metal) were characterized using complementary analytical methods (FEG-SEM, TEM, SIMS, optical microscopy). On the one hand, the characterized external oxide layer is very close to the one observed on industrial nickel-base alloys, hence validating the use of such model alloys. On the other hand, both free oxygen and oxides have been detected at grain boundaries several micrometers under the metal/oxide interface. Implications of such a finding on the involved transport mechanisms for oxygen and the intergranular stress corrosion cracking resistance of nickel-base alloys are then discussed.

Introduction

Environmentally-induced intergranular stress corrosion cracking (IGSCC) is known to be a damaging mode in number of nickel-base alloys used in pressurized water reactors (PWR) of nuclear power plants [1-5]. Alloy 600 has been studied intensively because of the widespread problems encountered with steam generators tubing and other components [2,3,5]. In spite of numerous studies, the mechanism that controls IGSCC in nickel-base alloys is still controversial [6-9]. However, evidence for an internal and/or intergranular embrittlement of polycrystalline Ni-alloys by oxygen already exists [10]. It has also been shown that alloys 600 and 690 both exhibit an inner chromium rich oxide layer (Cr rich spinel/Cr_2O_3) and a chromium depleted underlying metal layer after exposure to PWR primary water [10,11].

The continuous character of that inner chromium rich oxide scale is also known to depend directly upon the experimental parameters, such as surface preparation, temperature, pressure and chemical composition of the aqueous solution, as well as the chemical composition of the alloy. Indeed, as oxidation/dissolution phenomena occur during the growth of oxide scales, all under-layers (e.g. chromium depleted area, base metal) could then be exposed to a corrosive medium if the chromium rich oxide layer is discontinuous. It would be then relevant to study the behavior of such layers exposed to PWR primary water at 360°C. In addition, in order to ensure the development of a continuous protective Cr rich spinel/Cr_2O_3 oxide scale, hence lowering IGSCC sensitivity, the

chromium content of nickel-base alloys has been increased; this has led to the industrial replacement of alloy 600 (which contains ~15 wt% Cr) by the alloy 690 (~30 wt% Cr).

In addition, it is worthy to notice that the chromium gradient induced by oxidation has also a mechanical impact on the alloy grains. Indeed, the migration of chromium atoms towards the surface throughout the lattice generates a contraction of alloy grains, hence stressed grain boundaries. As the characterizations are made at room temperature after exposure to primary media, one should also take into account the difference of thermal expansion coefficient between the oxide scale and the underneath layers. Those last points are not investigated in the present work.

To date, the origin of the positive effect of chromium content on IGSCC sensitivity is not very well understood. Thus, the aim of this study was to perform a fine characterization of the oxide scales (nature, protective aspect, brittleness …) developed in simulated primary water on Ni-Fe-Cr ternary alloys representative of the chemical composition of chromium depleted layers observed on industrial alloys. The objective was to experimentally validate internal and/or intergranular oxidation by using different characterization techniques, from optical and electron microscopy observations to secondary ion mass spectrometry (SIMS) and help to improve understanding of both embrittlement mechanisms and the positive chromium effect.

Materials and Experimental Procedures

Model Ni-Fe-Cr ternary alloys used in this study were prepared by the research centre of Imphy Alloys with a strictly controlled processing route. Two different alloys were obtained by vacuum induction melting. Their nominal composition is given in Table 1.

Table.1 Chemical composition of Ni-Fe-Cr ternary alloys [weight %]

Heat	C	Cr	Fe	Ni
NiFe15Cr5	0.025	5.15	15.13	Bal.
NiFe10Cr10	0.027	10.2	10.39	Bal.

In order to keep the compositions as close as possible to industrial alloys, the concentrations of alloying elements, such as Al, Cu, Mn or Ti for example, were maintained within the specifications of alloys 600 and 690. The cast ingot was hot rolled down to the thickness of 5 – 6 mm. The microstructure of the model alloys was characterized by equiaxed small grains (ASTM grain size number = 8 – 9) and very few carbides (Fig. 1). For each heat, coupons were machined from the plates by milling in the form of rectangular bars 30 mm long, 20 mm width and 5 mm thick. The standard surface preparation of coupons consisted of grinding their surface down to SiC paper grade 1200. During and after these preparation steps, the coupons were ultrasonically cleaned in acetone, ethanol and pure water.

Exposures of the alloys to simulated PWR primary water were carried out in a static autoclave at 360°C for 50h, 300h and 1000h. PWR primary water was simulated by deionized and deaerated water to which was added 1200 ppm of boric acid and 2 ppm of lithium hydroxide. The partial pressure of hydrogen was set to 0.3 bar using a Pd-Ag membrane.

The morphology and microstructure of the corrosion products were characterized using a field emission gun scanning electron microscope (FEG-SEM) LEO 1530 operating at voltages from 100V to 30kV. Chemical analyses were performed in the SEM with an energy dispersive X-ray spectroscopy (EDX) system (Oxford Inca Energy). Transmission electron microscope (TEM)

characterization and EDX analyses were performed on cross-sections using the conventional preparation method (sandwich slices, dimpler, ion milling). A JEOL JEM 2010 microscope operating at 200 kV from the TEMSCAN service of the Paul Sabatier University, Toulouse was used. Note that, due to the difficulties in quantifying oxygen using EDX methods, the oxygen signal was not used for determining the composition of oxides (the percentages given in oxides correspond to the ratio of metallic cations).

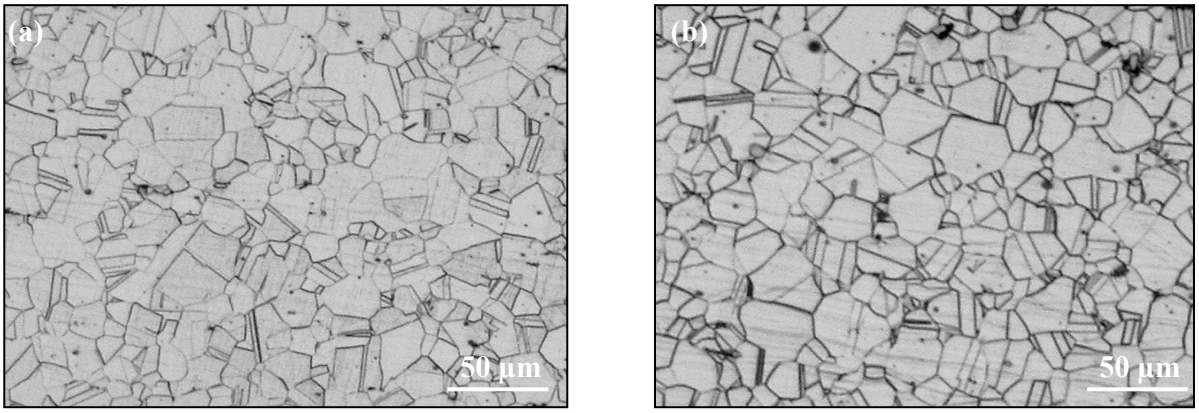

Fig. 1. Microstructure observed by SEM of studied model Ni-Fe-Cr ternary alloys after etching: (a) the 5% and (b) the 10% chromium alloys.

Local determinations of chemical composition by SIMS were performed using a CAMECA IMS 4F/6F instrument. Resistive Anode Encoder (RAE) mode was selected on the SIMS with an analyzed zone diameter of 30 µm. However, the total area of the abrasion zone was 150 x 150 µm². The RAE mode enables 2D-basic maps of oxygen and the main constitutive metallic elements of the alloy (Ni, Fe, Cr …) to be collected throughout the abrasion of the specimen. Cs^+ ions were used in order to reduce the "matrix effect". If M is the considered metallic element, the intensity of the collected M^+ secondary ions signal is strongly influenced by all other metallic cations with frequent aberration phenomena. It is no longer a problem if CsM+ metallic cation are collected; hence the use of the Cs+ ions source. The calibration of the abrasion rate for the specific material and operating conditions has been previously performed [10] by measuring the depth of different cavities using optical interferometry. Consequently, the collected data for the basic elemental maps can be both plotted versus time and/or depth.

In order to avoid roughness of the oxide scale influencing the definition of the location of the metal/oxide interface and to ensure highest sensitivity for crucial elements, particularly oxygen, SIMS analyses were also performed by abrading the metal from the underside of the oxide scale (so-called "Reverse mode"). For this purpose, specific specimens were prepared by mechanical polishing according to a procedure published previously [10].

In order to assess the accuracy of such a SIMS specimen preparation for both preventing roughness effects from affecting the SIMS analyses and determining precisely the thickness of the different layers and/or the length of intergranular oxide penetrations, complementary optical microscope characterizations were made as shown in Fig. 2.

A coupon of each model Ni-Fe-Cr alloy was cut into two parts after exposure to simulated primary water. One of them was analyzed by SIMS using the "Direct mode" (e.g. the abrasion of the specimen started from the outer surface of the oxide layer) whereas the second one was observed by optical microscopy (OM) after several polishing steps using a colloidal silica suspension (OP-S

Suspension ™ Struers). The polishing depth of each step was determined by the reduction of the diagonal length of four $HV_{1000/15s}$ hardness indentations arranged in a square of 1cm width. The comparison of depths given by the two methods shows conclusively that the SIMS data is reliable and has good accuracy for determining the depth of oxidation affected scale (e.g. external oxide layers, underlying scale and base metal affected by intergranular oxide penetrations).

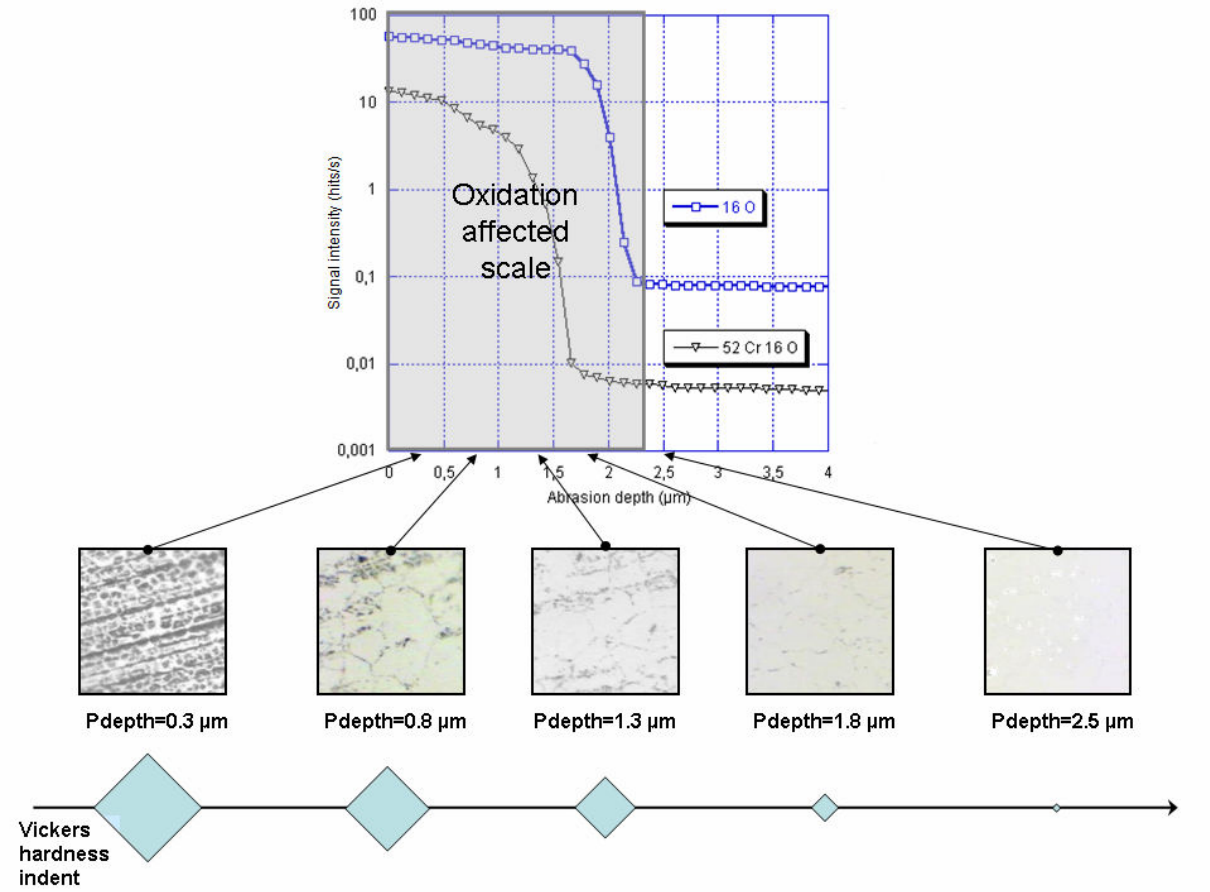

Fig. 2. Comparison between SIMS data and OM micrographs to compare and validate the calibration of ionic abrasion depth (SIMS) by a mechanical polishing depth (oxide penetration depth given by Vickers hardness indentation as shown above).

Results

Ten coupons of each model ternary alloy were characterized by STEM and SIMS after exposure to PWR primary medium at 360°C for 50h, 300h and 1000h. Two extra coupons of both the as-received heats were analyzed by SIMS in order to determine the average response of the technique for each element in the studied materials before the corrosion tests.

Table.2 Characteristics of the oxide layers appearing on Ni-Fe-Cr ternary alloys.

Heat	Maximum size of big crystallites	Composition of big crystallites	Maximum % of chromium in the inner layer[1]
NiFe15Cr5	Less than a µm	2 types: $NiFe_2O_4$ and Ni rich (78% Ni, 16% Fe, 6%Cr)	24
NiFe10Cr10	Less than a µm	35% Ni, 25% Fe, 40% Cr	70

[1]This percentage corresponds to the fraction of chromium among all the metallic cations excluding oxygen which was not quantified.

Structure of the oxide layer. The microstructure of the external oxide scale developed in simulated primary water on coupons was first examined by SEM. Both Ni-Fe-Cr ternary alloys exhibited a distribution of small crystallites as illustrated in Fig. 3. The size of these small crystallites was very similar for the two synthetic alloys of about 1 µm. EDX analyses showed two types of crystallites (Table 2), some nickel rich and also probably $NiFe_2O_4$ spinels (indicated by white arrows in Fig. 3).

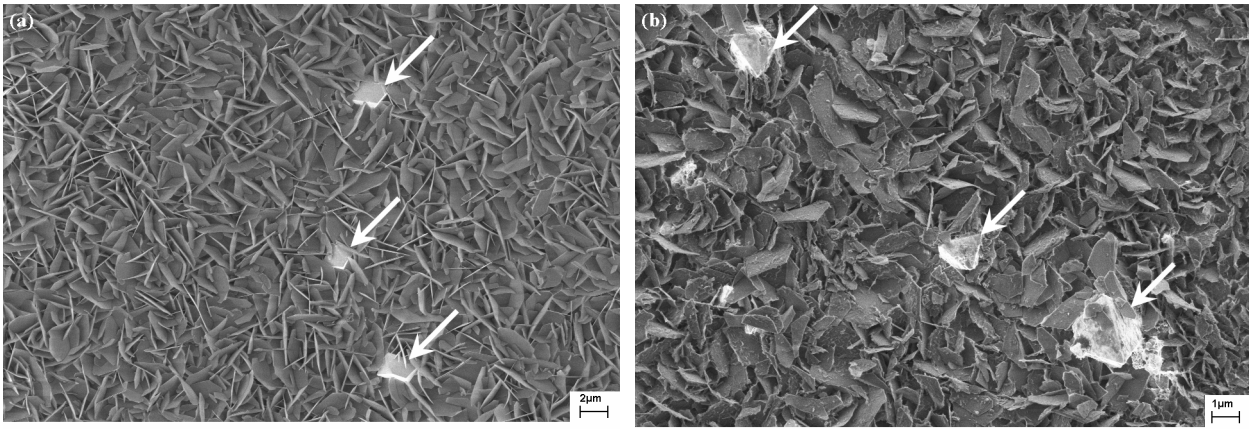

Fig. 3. SEM observation of the oxide scale developed after exposure to simulated primary water after 1000h at 360°C on (a) the 5% and (b) the 10% chromium model alloys. White arrows indicate Ni/Fe spinels.

The oxide scales were observed in cross-section by TEM in order to examine the different layers that composed the scale and also to analyze the composition of those layers more accurately than in the SEM. Fig. 4 shows an example of the whole structure of the oxide on the two studied alloys. The two kinds of crystallites observed by SEM were seen at the outer surface. The average thickness was about 100 nm. The layer appears not to have been a compact continuous one but instead was formed of discrete separated grains. Crystallite size was about 50 nm for the smallest ones whereas it ranged from 300 to 700 nm for the biggest ones, which corroborates the SEM observations. Another layer of very small oxide grains can also be distinguished underneath the crystallites. The thickness of this layer was around 10 nm and seemed to be quite constant. The layer appeared to be compact and continuous. The external oxide crystallites seemed to be embedded in this layer. EDX analyses showed that this inner oxide was chromium rich whereas the zone under the metal/oxide interface was chromium depleted over a distance of a few tens of nanometers (Fig. 5). Note that the level reached by chromium in the inner layer differed with the chromium content of studied alloys: 24 wt% for the 5% chromium model alloy and 70 wt% for the 10% chromium alloy. Furthermore, the tested times of exposure to simulated PWR primary medium

led to the same oxide layers with no noticeable difference in terms of dimensions and/or chemical composition. However, although the SEM and TEM data were in very good agreement, there was no evidence of intergranular oxidation and/or oxygen penetration in the underlying metal.

SIMS characterization of the metal/oxide interface and the underlying metal. In order to investigate if oxidation was present deeper inside the alloys than revealed by optical and electron microscopy, chemical analyses of the coupons were performed by SIMS both in the "Direct mode" and the "Reverse mode", as explained on Fig. 6. 2D-basic oxygen maps were collected in both abrasion modes and clearly demonstrated that oxygen penetrated over quite large distances into the metal (~ 10 µm). It is also interesting to note that this penetration of oxygen was not uniform but localized at grain boundary triple lines. Furthermore, the exposure time slightly modified the affected depth (9 µm after 50h and 12 µm after 1000h).

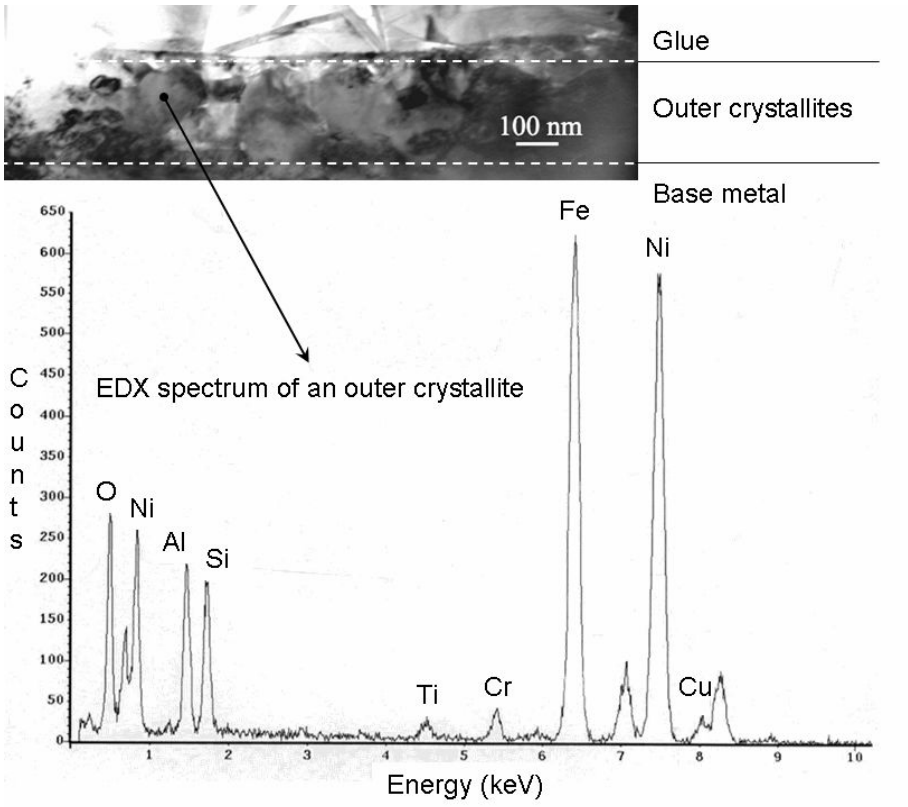

Fig. 4. TEM cross-section of the oxide scale developed after exposure to simulated primary water for 1000h at 360°C on the 5% chromium alloy and example of EDX analyses.

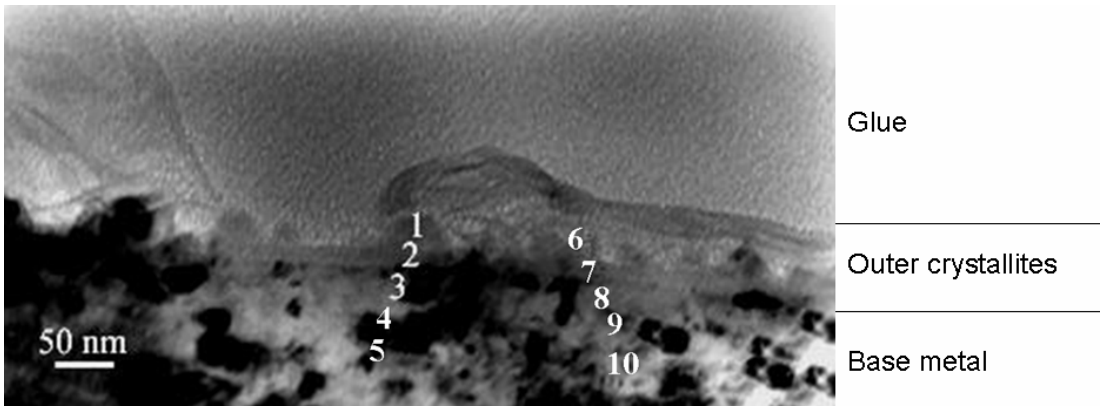

Fig. 5. TEM cross-section of the oxide scale developed after exposure to simulated primary water for 1000h at 360°C on the 10% chromium alloy and characterization of the chromium gradient by EDX analyses.

EDX analysis number	1	2	3	4	5	6	7	8	9	10
% of nickel[1]	36	17	50	79	81	34	22	64	83	78
% of iron[1]	26	13	11	16	10	25	16	13	10	12
% of chromium[1]	38	70	39	5	9	41	62	23	7	10

[1]These percentages correspond to the fraction of the considered element among all the metallic cations excluding oxygen which was not quantified.

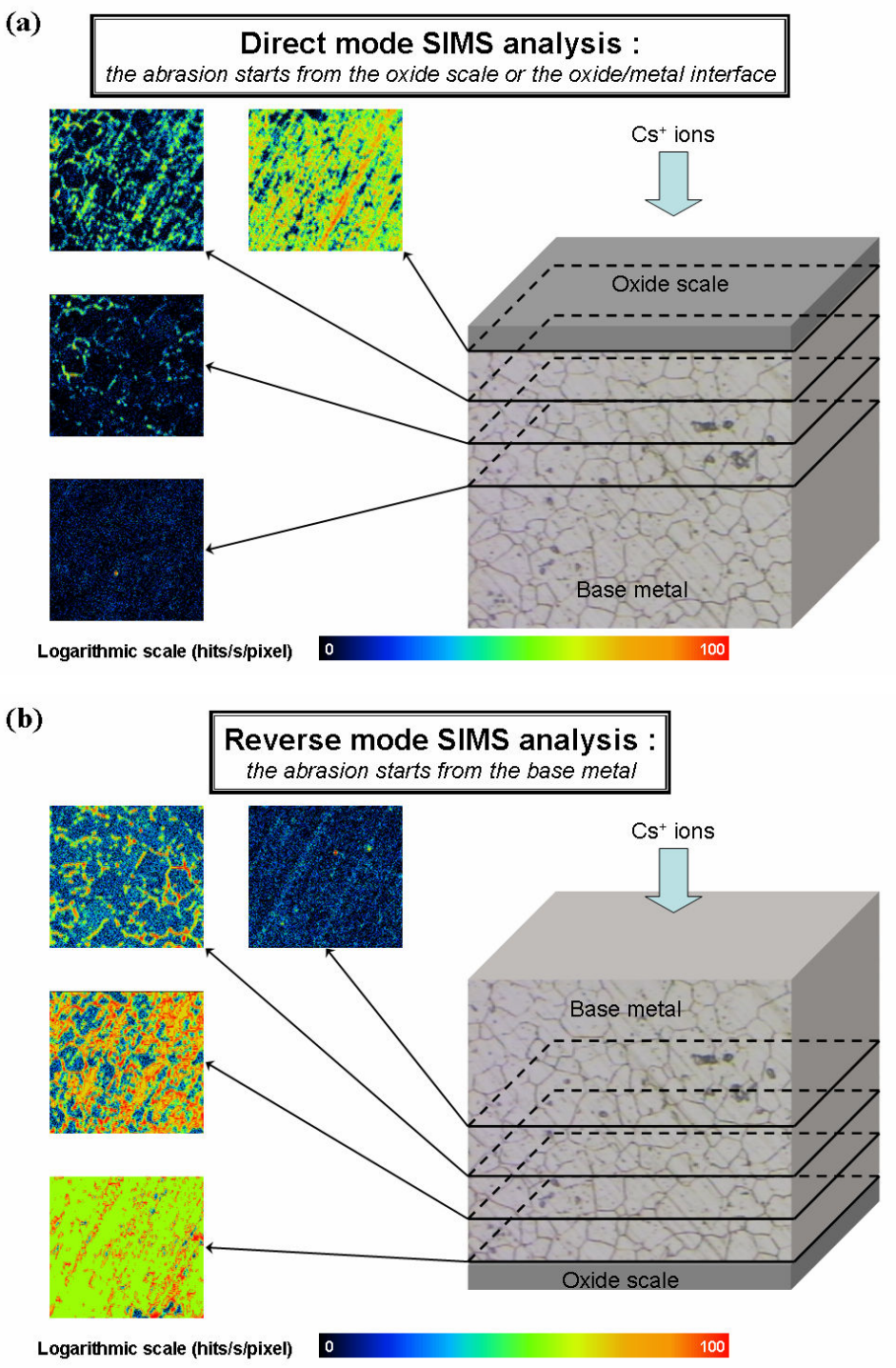

Fig. 6. Schematic explanation of the two kinds of SIMS abrasion modes: (a) Direct mode, (b) Reverse mode and examples of 2D-basic oxygen maps parallel to the metal/oxide interface obtained with the Resistive Anode Encoder (RAE) mode. The localization of oxygen throughout the analyzed specimen is very similar for both abrasion modes.

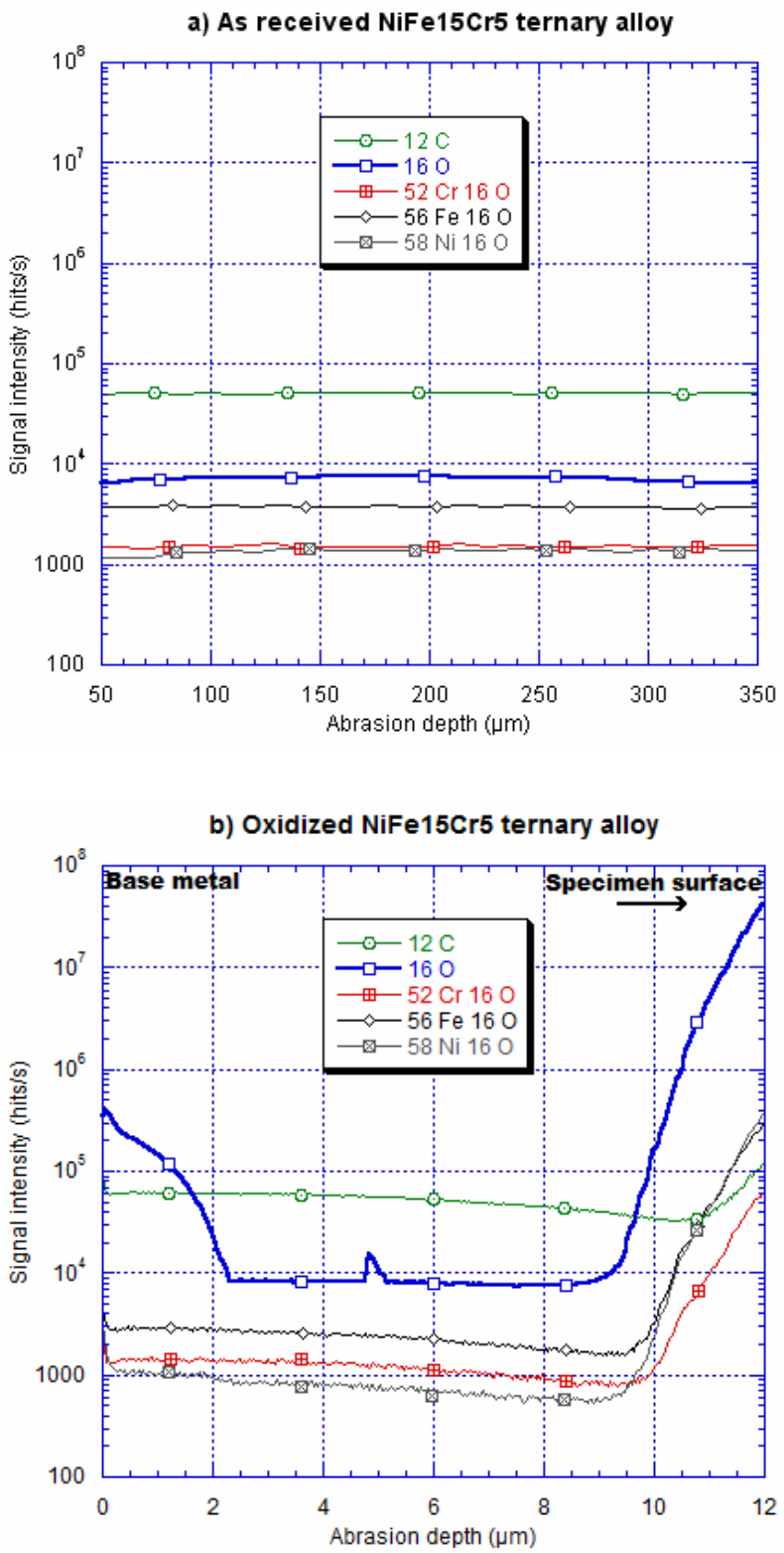

A M16O curve (with M=52Cr, 56Fe or 58Ni) corresponds to the signal intensity evolution of the oxidized form of the considered M metallic cation plotted versus abrasion depth.

Fig. 7. Comparison of SIMS profiles obtained for the 5% chromium model alloy before (a) and after (b) exposure to simulated primary water for 1000h at 360°C.

a) Reprocessed 2D basic oxygen maps parallel to the metal/oxide interface (RAE mode) to obtain a 3D reconstruction of the analyzed sample. Above and on the right of that 3D rebuilt sample, 2D cross sections perpendicular to the metal/oxide interface – Localization of the two profiles showed below.

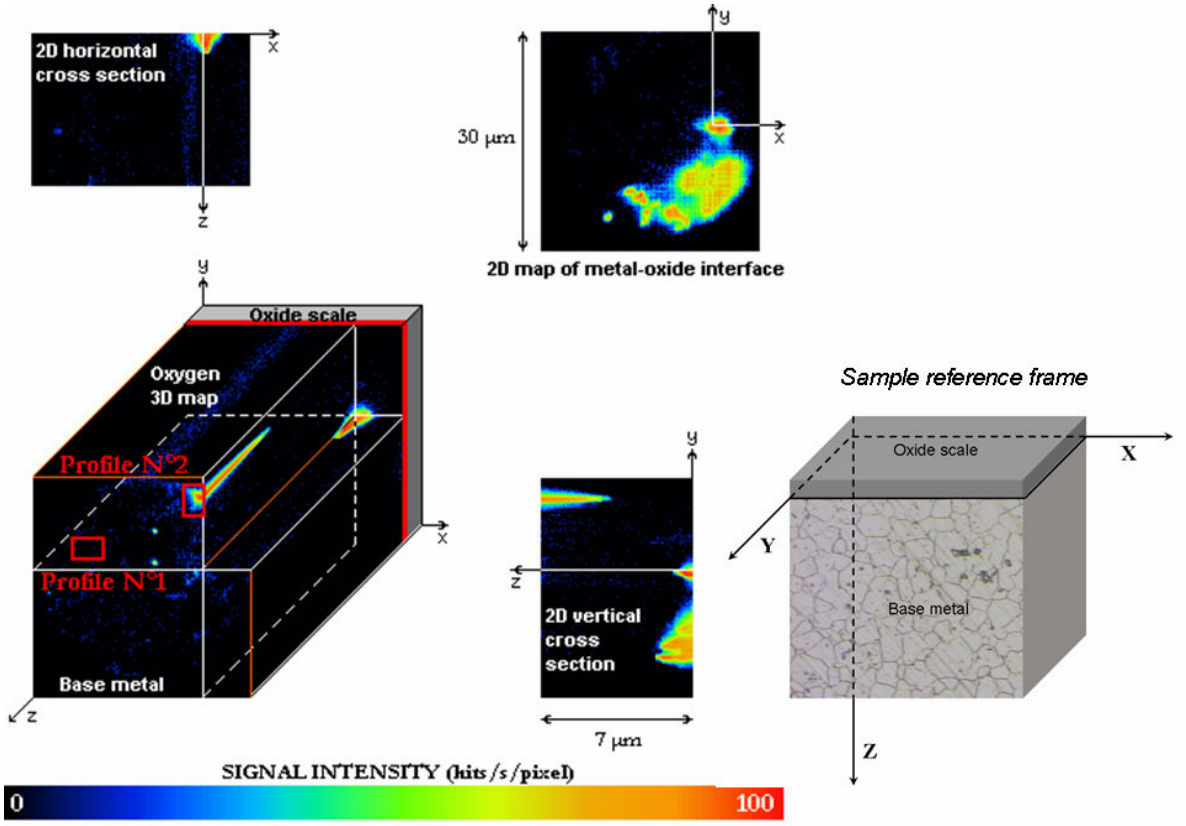

b) Comparison of SIMS profiles obtained for the base metal (profile N°1) and for the oxygen penetration area (profile N°2). See the 3D rebuilt sample above for the localization of the analyzed areas.

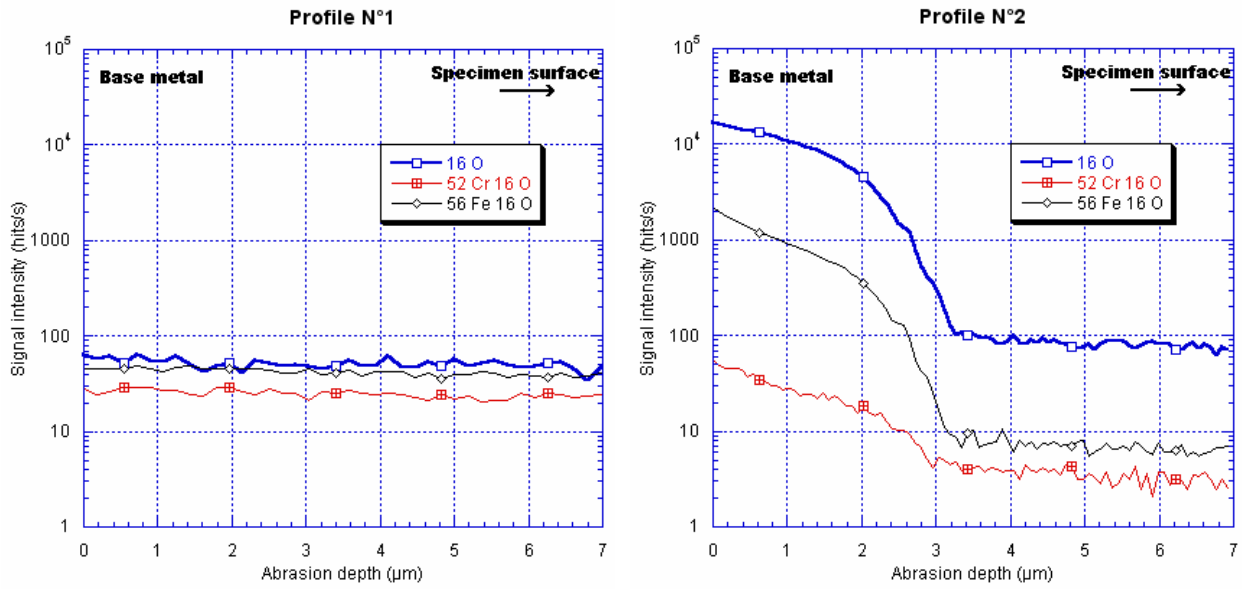

A M16O curve (with M=52Cr or 56Fe) corresponds to the signal intensity evolution of the oxidized form of the considered M metallic cation plotted versus abrasion depth.

Fig. 8. Evidence of oxygen penetration under the oxide scale for the 10% chromium model alloy after exposure to simulated primary water for 1000h at 360°C.

SIMS chemical analyses were also made for each ternary alloy before and after exposure to simulated primary water in the "Reverse mode" in order to measure more precisely oxygen and oxide distribution at the vicinity of the metal/oxide interface. The comparison of SIMS profiles in Fig. 7 conclusively demonstrates that the oxygen already detected on the 2D-basic maps presented in Fig. 6 was not linked to the preparation of the model ternary alloys but directly linked with the exposure of the coupons to simulated PWR primary water. The signal intensities of each element remained quite constant for the non exposed coupons. The carbon signal intensity is given in order to assess whether the detected increase of the oxygen signal intensity for the oxidized coupons (Fig. 7(b)) was due to the reaction of oxygen with carbides; no oxidation of carbides was highlighted. Profiles in Fig. 7(b) confirmed the thickness and the chemical composition of the oxidation affected layer, as determined by optical and electronic microscopy. The average thickness of the oxidation affected scale was about 10 μm. The outer oxide layer was made of mixed oxides (mainly Ni-rich oxides) whereas the inner layer was chromium rich oxide. However in the "Reverse" scans, the first ionic signal to increase was surprisingly identified as oxygen alone without any correlation with other elemental signals. The extent of this zone where oxygen penetrated beneath the oxide reached 200 nm. Small "islands" of oxygen were detected up to 12 μm below the metal/oxide interface with a width of less than a micrometer.

The SIMS data are summarized in Fig. 8(a) showing 3D reprocessed RAE maps to "rebuild" the analyzed volume of the coupon. Contrary to STEM observations which remain local and/or 2D representations of the polycrystal, SIMS analyses provide more volumetric data, with an average analyzed volume of about 30x30x10 μm^3. In addition, it is possible to generate SIMS profiles corresponding to selected 2D areas of the 3D reconstruction illustrated in Fig. 8(b). The obtained results are consistent with those of Fig. 7. Profile N°1 clearly shows that the exposure to simulated primary water had no consequence for the average signal intensities of each matrix element. However, if a quite small area around an oxygen penetration along the grain boundaries/triple lines is considered, a second kind of small "island" of oxygen can be observed in the underlying metal. This oxygen is not "free" but associated with the metallic elements (Cr and Fe). Another kind of "island" could be observed: oxygen associated with silicon and magnesium.

Discussion

The structure of the oxide layer developed from the examination of the model ternary alloys after exposure to simulated primary water is summarized in the sketch of Fig. 9. The outer scale was composed of two families of oxide grains, one in the form of discrete large crystallites ($NiFe_2O_4$ spinel oxides) and the other, which apparently covered the whole surface, made of smaller grains of a mixed oxide of nickel, chromium and iron of average thickness of 50 nm. The oxide scale was not compact and was judged to be non-protective. Such an observed oxide structure is in good agreement with previous studies [10-13].

The different models developed to describe the corrosion behavior of such alloys in pressurized pure water at high temperature can be considered in the light of these results. All of them are based on an original one proposed by Evans [14] for the corrosion of iron in caustic solution that assumes a duplex microstructure for the growing oxide scale. That duplex structure was observed in the present work. A mechanism of growth involving dissolution and precipitation can be supported to explain such an observed oxide structure [14,15]. In addition, another thin, compact and continuous inner layer made of Cr rich spinel/Cr_2O_3 oxide was identified at the metal/oxide interface. This layer is assumed to be the first to be able to act as a barrier to further oxidation. This modifies the usual

duplex description of oxide scales. However, such a structure has already been observed on a similar alloy [16]. Furthermore, it should also be kept in mind that exposure to PWR primary water at 360°C affects the underlying metal; a chromium depleted layer is present over a few tens nanometers under the inner chromium rich oxide scale. This phenomenon could be linked with what is well known at higher temperatures (800°C – 1200°C): nickel-chromium alloys exhibit sensitivity to intergranular and internal oxidation for chromium contents lower than 10% [17]. Moreover, the formation of the chromium depleted zone in the metal is related to that of the chromium rich inner oxide layer. As a gradient of chromium concentration is observed, it is commonly assumed that a chromium rich oxide layer is formed by the diffusion and selective oxidation of chromium atoms. Such a mechanism has been studied [15,18] and implies the injection of vacancies into the material beneath the oxide scale [18]. Up to now, the oxide layers grown on nickel-base alloys after exposure to PWR primary medium have been described as having a duplex structure formed by an inner Cr-rich layer and an outer layer consisting of two well-defined families of crystallites. A third area can be identified as a consequence of the corrosion phenomena, namely the chromium depleted layer beneath the oxide. On average, the overall thickness of the corrosion scales was about a micrometer.

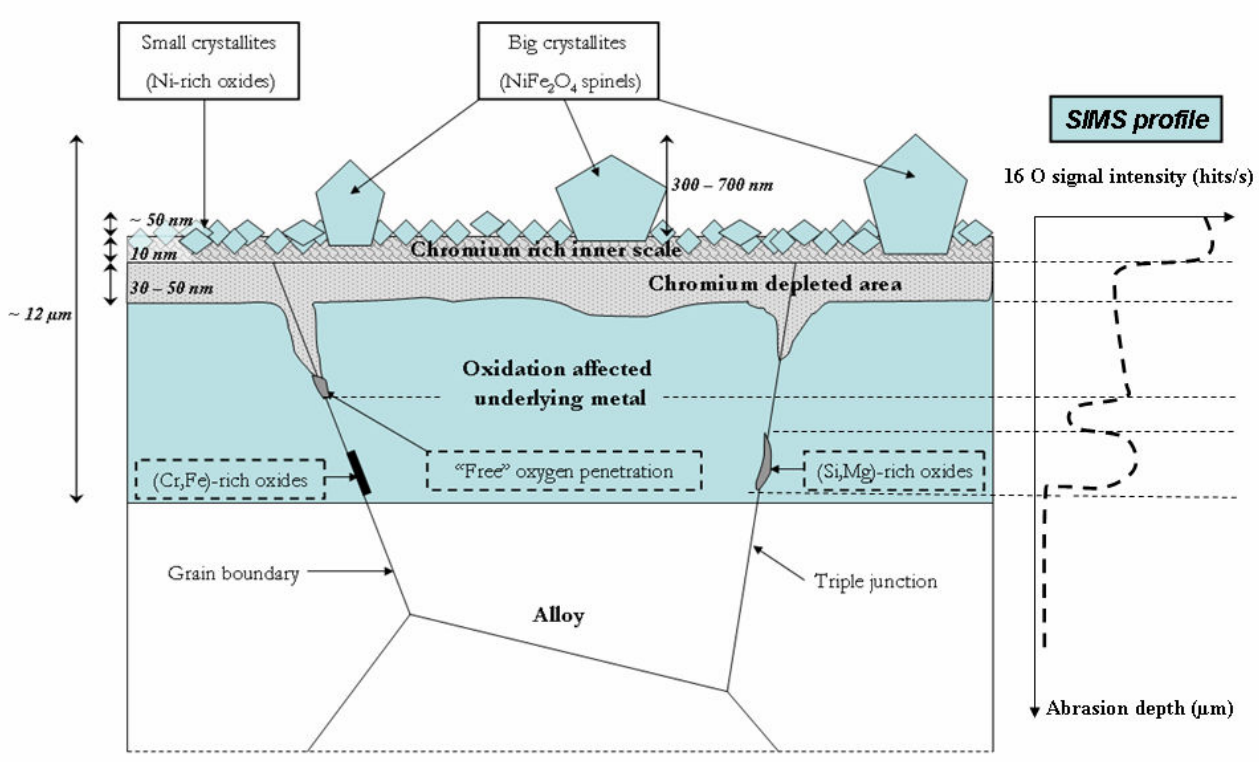

Fig. 9. Sketch summarizing the oxide film structure on model Ni-Fe-Cr ternary alloys and intergranular penetrations after exposure to simulated primary water for 1000h at 360°C.

One of the striking results of the present work is the observation of the presence of oxygen in the alloys to several micrometers under the oxide layer. Preferential oxygen penetration along the grain boundaries/triple lines was observed, which is consistent with an intergranular/internal oxidation phenomenon. Indeed, two types of small "islands" of oxygen were detected on both ternary model alloys, independent of their chromium content is. In one case, the small "islands" were related to the formation of oxides of the metals/impurities present in the matrix (e.g. mainly chromium oxide or silicon/magnesium oxide). "Free" oxygen atoms dissolved in the metal matrix were also observed

upstream to the intergranular oxide penetration (IOP) along grain boundaries/triple lines. The affected depths reached more than 10 μm into the alloy suggesting an oxygen transport mechanism applying over large distances. An outstanding question remains as to whether oxygen penetrates along grain boundaries before or while the continuous protective Cr rich spinel/Cr_2O_3 oxide layer is forming. For the three tested times of exposure to PWR primary medium, the affected depth remains quite important and a kinetic study for shorter times (< 50 h) has to be performed to collect data so as to describe precisely the very first steps of the corrosion phenomenon.

Intergranular oxide penetrations remain difficult to explain by diffusional mechanisms, even those already observed at higher temperatures [10,11,19]. For example, by extrapolating to 300°C the results of Bricknell and Woodford [20] for high-temperature diffusion of oxygen in nickel, the required time for oxygen to penetrate as far as 10 nm is several years. However, intergranular embrittlement of grain boundaries by oxygen has been attributed to a possible accelerated "transport" of free oxygen as compared to the normal bulk diffusion coefficients [21-23]. According to Scott [21], the applied mechanical loading and/or the porous structure of crack oxide can increase oxygen diffusion rates significantly at grain boundaries. This embrittlement can also be attributed to the accelerated transport of oxygen by vacancy injection at grain boundaries [23]. This phenomenon allows the formation of oxides in the grain boundaries and so contributes to their embrittlement. Such an assumption is in agreement with SIMS profiles presented in Fig. 8b.

To sum up, evidence of both intergranular and internal oxidation of synthetic ternary alloys has been observed, including the presence of small "islands" of oxides deep under the metal/oxide interface. As a continuous protective Cr rich spinel/Cr_2O_3 oxide layer forms on both alloys, the "free" oxygen observed along grain boundaries/triple lines in the vicinity of IOP may result from a massive penetration of oxygen during the very first steps of oxidation (e.g. as long as the chromium rich layer is not continuous and thick enough). The detected small "islands" of chromium/iron and silicon/magnesium oxides may have been formed subsequently, so as to reduce the amount of free oxygen in the alloy to reach a pseudo-equilibrium state. Finally, whatever the involved mechanisms could be for the formation of small oxide "islands", they have to be considered as "damaging spots", in good agreement with what was already known in term of interface embrittlement mechanisms [24-28]. Consequently, it would be then better to consider an "oxidation affected layer" rather than the classical "oxide scale thickness" to evaluate the depth of alloy affected by the corrosion/oxidation processes. This is all the more true since it has been established that the metal/oxide scale can no longer be described as a planar interface parallel to the initial surface because both oxide and oxygen penetrations are deeper along grain boundaries/triple lines.

Finally, the complete set of observations of the present study can be easily conciliated by considering transport phenomena based on bonding effects between vacancies and oxygen atoms [18]. Such a binding effect has been observed recently in a study of the high-temperature oxidation of pure nickel [23,29]. The selective oxidation of chromium produces vacancies close to the metal/oxide interface which are able to diffuse along grains boundaries toward the bulk material driven by the concentration gradient. This migration accelerates the diffusion of chromium in the opposite direction, hence accelerating chromium depletion. Transport of interstitial species, including oxygen, is expected due to a binding effect between atoms of small size and vacancies. Moreover, the vacancy concentration is gradually reduced as a compact and continuous Cr rich spinel/Cr_2O_3 layer grows until it becomes zero. This mechanism is all the more probable as the oxidation took place at 360°C and the mobility of the couple vacancy-oxygen atom should be much higher than the one of oxygen alone and similar to the one of a vacancy alone [29,30]. Indeed, in the

vicinity of a vacancy, the activation energy for oxygen diffusion is very small. As a consequence, all the results obtained in this study, after comparison with former proposed models, tend to plead for an oxidation mechanism based on internal and intergranular oxidation [21,31], leading to an embrittlement of grain boundaries.

Conclusion

The corrosion products on synthetic ternary Ni-Fe-Cr alloys were characterized by electron microscopy (SEM and TEM) and chemical analysis (EDX and SIMS) after exposure to simulated PWR primary water at 360°C for 50h, 300h and 1000h. It was shown that the oxide scale is to be described as a triple layer and that only a thin chromium oxide layer is continuous and could be considered as a protective layer. Indeed, it was also shown that there exists a chromium depleted zone in the metal and that penetrations of oxygen under the oxide scale are evidenced by SIMS imaging. Oxygen was observed in solution and associated with chromium or silicon/magnesium along triple lines as far as 12 μm from the oxidized surface. All those facts are in good agreement with previously established experimental facts on industrial alloys, such as alloy 600 or alloy 690. As a consequence, using such coupled characterizations (e.g. STEM and SIMS) of model and/or industrial alloys after exposure to oxidizing environments seems to be of relevant interest to study the mechanisms involved in intergranular oxidation and oxygen enhanced crack growth.

References

[1] M.T. Miglin, H.A. Domian: J Mater Eng, Vol.9 (1987), p.113

[2] R.H. Jones, S.M. Bruemmer: Proceedings of the 1st International Conference on Environment-Induced Cracking of Metals, edited by R.P. Gangloff and M.B. Ives, NACE (1988), p.287

[3] G.S. Was: Corrosion, Vol.46 (1990), p.319

[4] M.O. Speidel, R. Magdowski: Proceedings of the 6th International Symposium on Environmental Degradation of Materials in Nuclear Power Systems – Water Reactors, edited by R.E. Gold and E.P. Simonen, TMS (1993), p.361

[5] P.M. Scott: Int J Pres Ves and Piping, Vol.65 (1996), p.255

[6] T. Magnin, F. Foct, O. de Bouvier: Proceedings of the 9th International Symposium on Environmental Degradation of Materials in Nuclear Power Systems – Water Reactors, edited by S.M. Bruemmer and F. P. Ford, TMS (1999), p.27

[7] P.M. Scott: Proceedings of the 9th International Symposium on Environmental Degradation of Materials in Nuclear Power Systems – Water Reactors, edited by S.M. Bruemmer and F. P. Ford, TMS (1999), p.3

[8] E. Andrieu, B. Pieraggi: Proceedings of the 2nd International Conference on Corrosion-Deformation Interactions CDI'96, edited by T.Magnin, Woodhead publishing (1996), p.294

[9] G. Was, D.J. Paraventi, J.L. Hertzberg: Proceedings of the 2nd International Conference on Corrosion-Deformation Interactions CDI'96, edited by T.Magnin, Woodhead publishing (1996), p.410

[10] F. Delabrouille, B. Viguier, L. Legras, E. Andrieu: Proceedings of the 6th International Conference on the Microscopy of oxidation (2005), p.115

[11] J. Panter, B. Viguier, J.M. Cloué, M. Foucault, P. Combrade, E. Andrieu: J Nuclear Materials, Vol.348 (2006), p. 213

[12] C. Soustelle, M., Foucault P. Combrade: Proceedings of the 9th International Symposium on Environmental Degradation of Materials in Nuclear Power Systems – Water Reactors, edited by S.M. Bruemmer and F. P. Ford, TMS (1999), p.105

[13] A. Machet, A. Galtayries, P. Marcus, P. Combrade, P. Jolivet, P.M. Scott: Surf Interface Anal, Vol.34 (2002), p.197

[14] U.R. Evans, J.N. Wanklyn: Nature, Vol.162 (1948), p.27

[15] J. Robertson: Corros Sci, Vol.32 (1991), p.443

[16] F. Carette, M.C. Lafont, G. Chatainier, L. Guinard, B. Pieraggi: Surf Interface Ana*l*, Vol.34 (2002), p.135

[17] C.S. Giggins, F.S. Pettit: Trans Met Soc AIME, Vol.254 (1969), p.2495

[18] E.P. Simonen, L.E. Thomas, S.M. Bruemmer: Corrosion 2000 (2000), p.226

[19] R.C. Newman, T.S. Gendron, P.M. Scott: Proceedings of the 9th International Symposium on Environmental Degradation of Materials in Nuclear Power Systems – Water Reactors, edited by S.M. Bruemmer and F. P. Ford, TMS (1999), p.79

[20] R.H. Bricknell, D.A. Woodford: Acta Metall, Vol.30 (1982), p.257

[21] P.M. Scott, M. Le Calvar: Proceedings of the 2nd International Conference on Corrosion-Deformation Interactions CDI'96, edited by T.Magnin, Woodhead publishing (1996), p.384

[22] R.H. Bricknell, D.A. Woodford: Metall Mater Trans A, Vol.12 (1981), p.425

[23] S. Pérusin, B. Viguier, D. Monceau, L. Ressier, E. Andrieu: Acta Mater, Vol.52 (2004), p.5375

[24] W. Carpenter, B.S.J. Kang, K.M. Chang: Superalloys 718, 625, 706 and various derivatives, edited by E.A. Loria, TMS (1997), p.679

[25] J. Rösler, S. Müller: Scripta Mater, Vol.40 (1997), p.257

[26] C.F. Miller, G.W. Simmons, R.P. Wei: Scripta Mater, Vol.42 (2000), p.227

[27] C.F. Miller, G.W. Simmons, R.P. Wei: Scripta Mater, Vol.44 (2001), p.2405

[28] R. Molins, G. Hochstetter, J.C., Chassaigne E. Andrieu: Acta Mater, Vol.45 (1997), p.663

[29] E.H. Megchiche, S. Pérusin, J.C. Barthelat, C. Mijoule: Phys Rev B, Vol.74 (2006), p.06411

[30] R.A. Johnson, N.Q. Lam: Phys Rev B, Vol.13 (1976), p.4364

[31] T.S. Gendron, P.M. Scott, S.M. Bruemmer., L.E. Thomas: Proceedings of the 3rd International Steam Generator and Heat Exchanger Conference, CNS (1998), p.389

High Temperature Corrosion and Protection of Materials 7
doi:10.4028/www.scientific.net/MSF.595-598

Kinetic Study of the Low Temperature Internal Oxidation of Nickel Based Model Alloys Exposed to PWR Primary Water
doi:10.4028/www.scientific.net/MSF.595-598.449